Failure Analysis of an Ammonia Refrigerant Condenser Tube

N.G. Muralidharan, R. Kaul, K.V. Kasiviswanathan, T. Jayakumar, and B. Raj

A detailed failure analysis was conducted on an ammonia refrigerant condenser tube component that failed catastrophically during its initial hours of operation. Evidence collected clearly demonstrated that the weld between a pipe and a dished end contained a sharp unfused region at its root (lack of penetration). Component failure had started from this weld defect. The hydrogen absorbed during welding facilitated crack initiation from this weld defect during storage of the component after welding. Poor weld toughness at the low operating temperature facilitated crack growth during startup, culminating in catastrophic failure as soon as the crack exceeded critical length.

Keywords
failure analysis, steel type API 5L gr. B, weld failure, welding

1. Introduction

CATASTROPHIC failure of an ammonia refrigerant condenser tube occurred within 3 h of its operation. The failed component was a 370 mm diam pipe (with a wall thickness of about 11 mm) with its end welded to a hemispherical dished end (with a maximum wall thickness of about 15.9 mm near the weld). The welded component formed the dead end of the pipeline. During its brief operating life, the component was filled with ammonia. The internal pressure was dropping from 0.1 MPa to the final pressure of 0.04 MPa, and the temperature was correspondingly decreasing from 270 to 241 K.

It was reported that the failed pipe had been welded to the dished end by shielded metal arc welding using AWS E 6013 flux-coated electrode with a recommended moisture content of less than 1%. Before being placed in operation, the welded pipe was hydrostatically tested at a pressure of 3.2 MPa and was deemed acceptable. No radiographic examination was carried out on the welded component before the hydrostatic test.

2. Materials of Construction

The materials of construction of the pipe and dished end were reported as API 5L grade B and A 234 (WPB) (equivalent to A106 grade B), respectively (Ref 1). The yield strength and ultimate tensile strength of these materials are reported as 241 and 414 MPa, respectively (Ref 2). Their nominal chemical compositions are given in Table 1.

3. Testing Procedure and Results

3.1 *Visual Examination*

The failed component is shown in Fig. 1. Figure 2 is a schematic that shows the extensive crack pattern on the component. On the diametrically opposite side of the main fracture location, a longitudinal crack running across the pipe-to-dished-end weld was also noticed. No sign of significant plastic deformation was associated with the failure. The weld joint exhibited nonuniform penetration. Moreover, the weld joint of the two components, which differed in thickness, had a sharp taper of 2 to 3 mm on the inner surface.

All fractured surfaces were associated with chevron marks. The directions of crack propagation, as indicated by the chevron marks, are schematically shown in Fig. 2. The fracture was initiated from two locations: zones I and II. The main crack propagated from zone 1 toward A and B in the longitudinal direction and then subsequently deviated in the circumferential direction, while a second crack propagated toward C. From zone II, another crack propagated in the longitudinal direction toward D. The fracture surface corresponding to location E shows evidence of failure by tearing. The partially separated part of the pipe, DECB, was deflected out with respect to the remaining part of the component, probably due to impact loading during final failure.

3.2 *X-radiographic Examination*

Radiographic examination of the circumferential weld of the failed component revealed lack of penetration throughout most of the weld length. A positive print of the X-radiograph is shown in Fig. 3.

3.3 *Fractographic Examination*

Fractographic examination of the fracture surfaces at low magnification revealed their brittle nature. The presence of chevron marks on the fracture surfaces (Fig. 4) indicated lack of ductility for the material as well as the direction of crack propagation. Both crack nucleation sites, as shown in Fig. 2,

Table 1 Nominal chemical compositions of materials of construction

Element	Nominal chemical composition, wt%	
	Pipe	Dished end
Carbon	0.25	0.30
Manganese	0.95	0.29-1.06
Sulfur	0.06 max	0.06 max
Phosphorus	0.05 max	0.05 max

N.G. Muralidharan, R. Kaul, K.V. Kasiviswanathan, T. Jayakumar, and **B. Raj,** Division for PIE & NDT Development, Indira Gandhi Centre for Atomic Research, Kalpakkam, India.

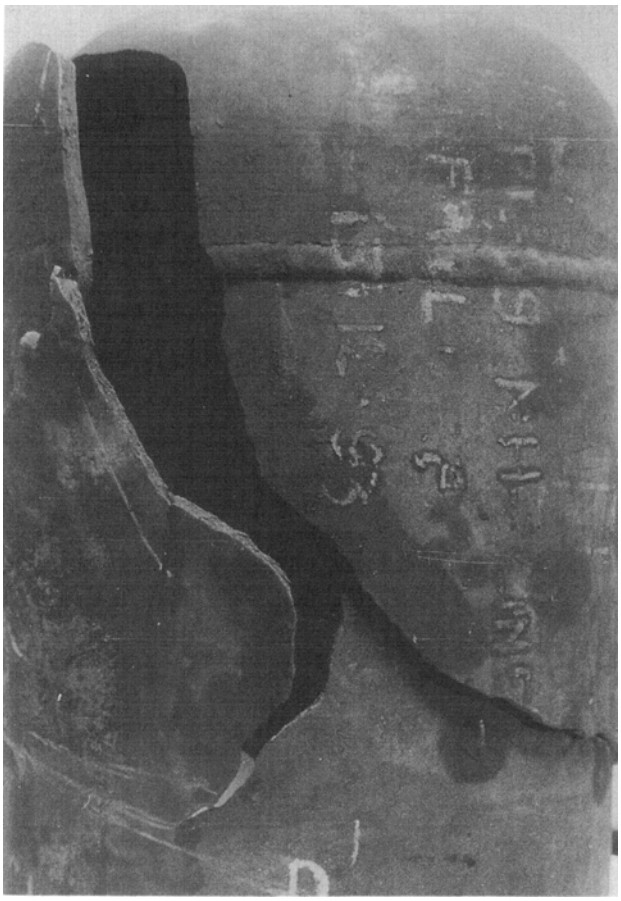

Fig. 1 As-received failed condenser tube

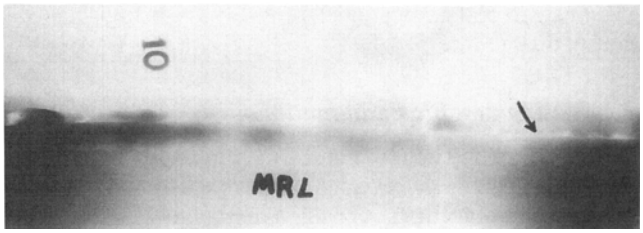

Fig. 3 Positive print of an x-radiograph of the pipe-to-dished-end weld showing area of lack of penetration

exhibited large regions of lack of penetration (Fig. 5). Several microcracks emanating from this area were also noticed. Near the crack nucleation zone, the fracture surface was found to be intergranular in nature (Fig. 6).

3.4 *Metallographic Examination*

Metallographic examination was carried out on specimens removed from the dished end and from the weld. The weld specimen was taken from the region close to the crack nucleation zone. The pipe material exhibited a ferrite-pearlite microstructure, while the dished end exhibited a banded structure of ferrite and pearlite. The weld microstructure consisted of a mixture of acicular ferrite, grain-boundary ferrite, and polygonal ferrite.

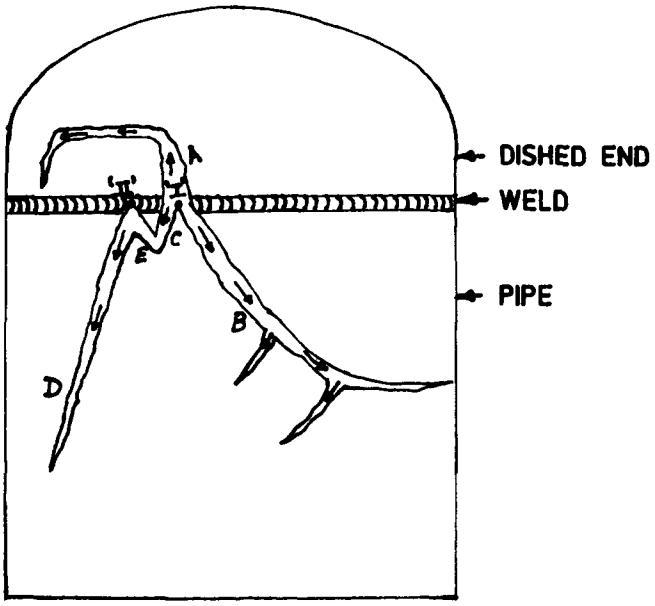

Fig. 2 Schematic showing directions of crack propagation, as indicated by chevron marks

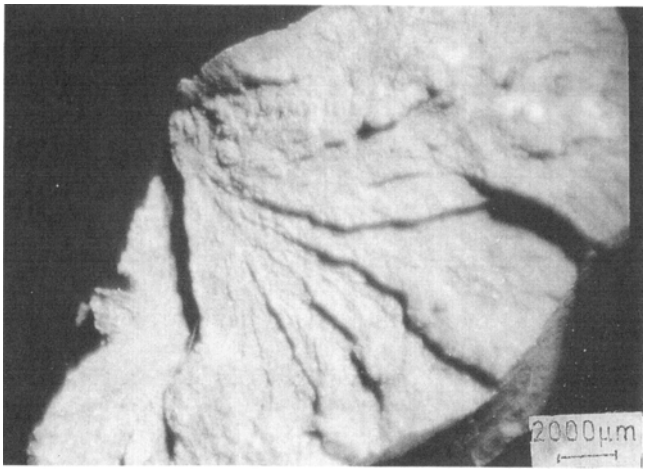

Fig. 4 Chevron marks on fracture surface

The weld specimen also exhibited an area of sharp lack of penetration. Figure 7 shows an intergranular crack emanating from this weld defect. This crack was seen to be propagating through inclusions (Fig. 8). A closer look at it and other cracks revealed that they initiated at inclusion sites (Fig. 9). Figure 10 shows blisters around the inclusions. These blisters would have been formed as a result of precipitation of molecular hydrogen at the matrix/particle interface. In addition, several cavities were present around the inclusions (Fig. 11). Energy-dispersive analysis of x-rays (EDAX) conducted on the inclusions revealed the presence of iron, manganese, aluminum, and sulfur, implying that the inclusions were composed of mainly MnS.

3.5 *Microhardness Measurements*

Microhardness measurements (using a 50 g load) carried out on polished specimens taken from pipe and dished-end ma-

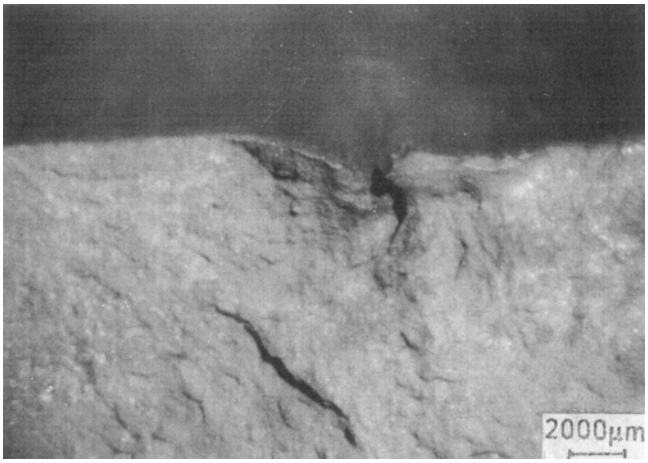

Fig. 5 Area of sharp lack of penetration at crack nucleation site

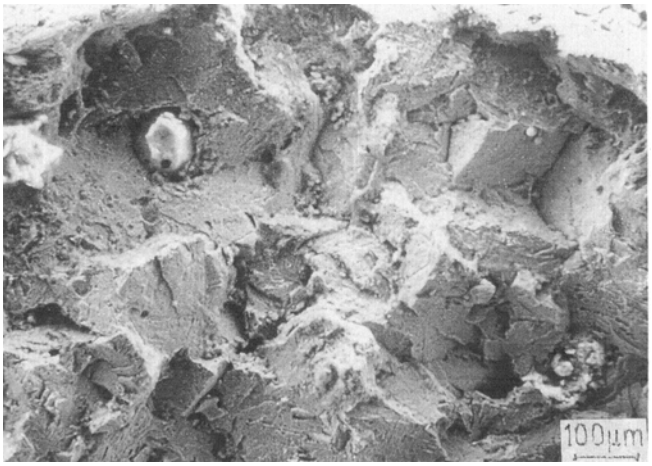

Fig. 6 Intergranular nature of fracture surface near crack nucleation site

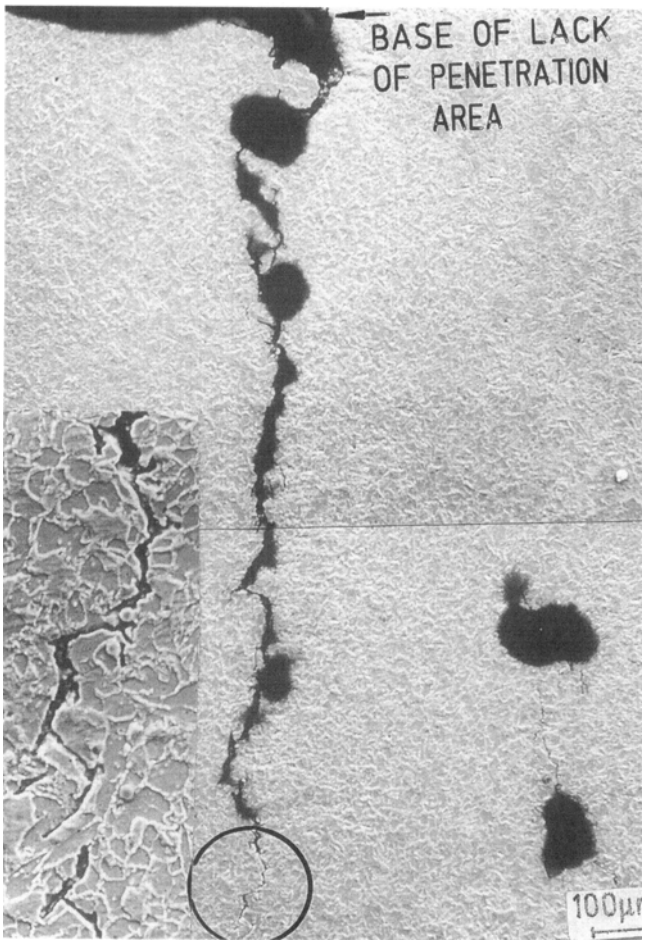

Fig. 7 Crack emanating from the base of the area of lack of penetration. The inset figure, a magnified view of the encircled region, shows the intergranular nature of cracking.

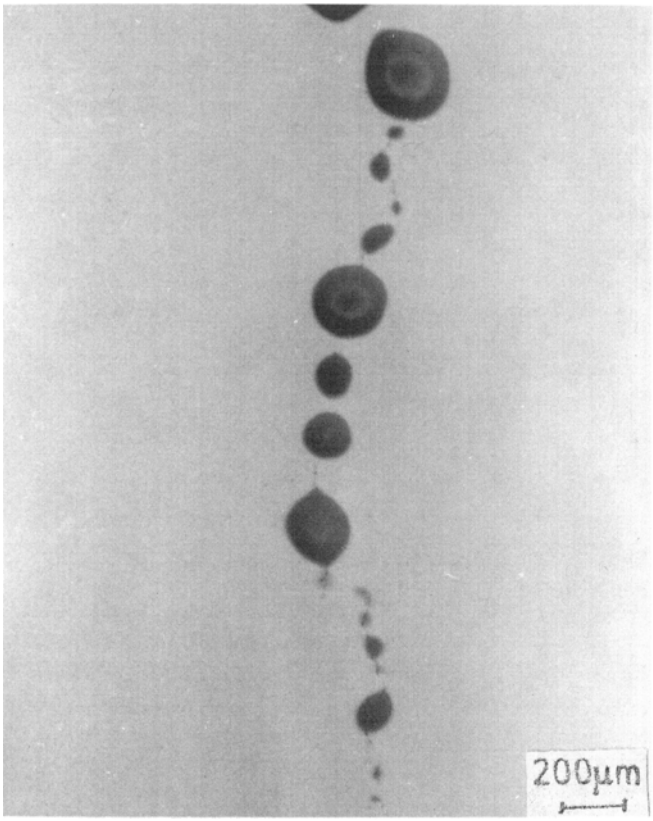

Fig. 8 Crack joining inclusions

terial indicated hardness values of 286 and 193 HV, respectively. The weld region of the failed component exhibited microhardness values of 260 to 290 HV in the top region of the weld, whereas the microhardness of the bottom region of the weld was in the range of 210 to 230 HV.

3.6 *Impact Testing*

To evaluate the low-temperature impact properties of the weld with respect to the base metal, subsize Charpy V-notch impact specimens (55 by 10 by 5 mm) were taken from the failed component. Dimensional details and the orientation (for specimens taken from the weld) of the subsize Charpy speci-

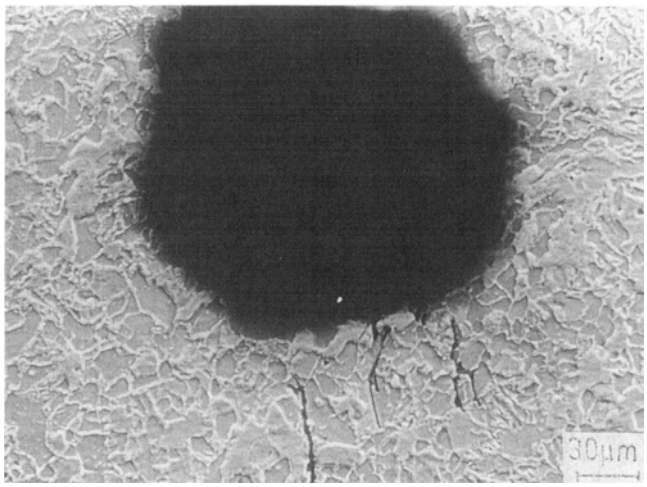

Fig. 9 Cracks emanating from inclusion sites

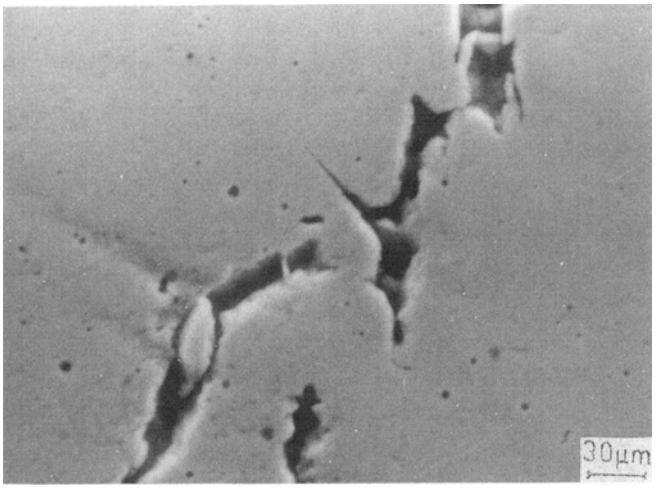

Fig. 10 Blisters around inclusions

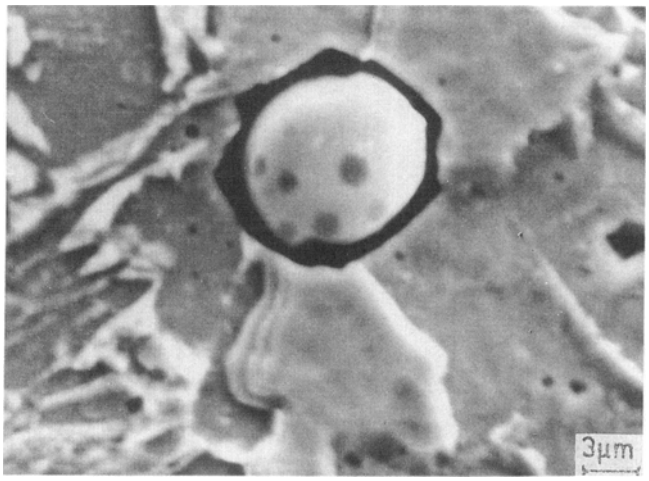

Fig. 11 Decohesion of inclusion/matrix interface

Table 2 Chemical compositions of materials of construction

Element	Chemical composition, wt %		
	Pipe	Dished end	Weld
Carbon	0.19	0.28	0.18
Manganese	0.52	0.54	0.44
Sulfur	0.03	0.01	0.02
Phosphorus	0.004	0.028	0.015

mens are given in Fig. 12 (Ref 3, 4). The tests were performed on a Tinius-Olsen model 358 J (Tinius-Olsen Testing Machine Co., Inc., Willow Grove, PA) impact machine with DYNATUP (GRC Instruments, Santa Barbara, CA) instrumentation, as per ASTM E 23 (Ref 3). The results of impact tests carried out on subsize Charpy specimens at different temperatures are presented in Fig. 13. Transition temperatures for subsize Charpy specimens from base metal and weld metal (using 0.25 J/mm^2 ligament area criterion, equivalent to 10 J for subsize specimens) were calculated as 210 and 247 K, respectively.

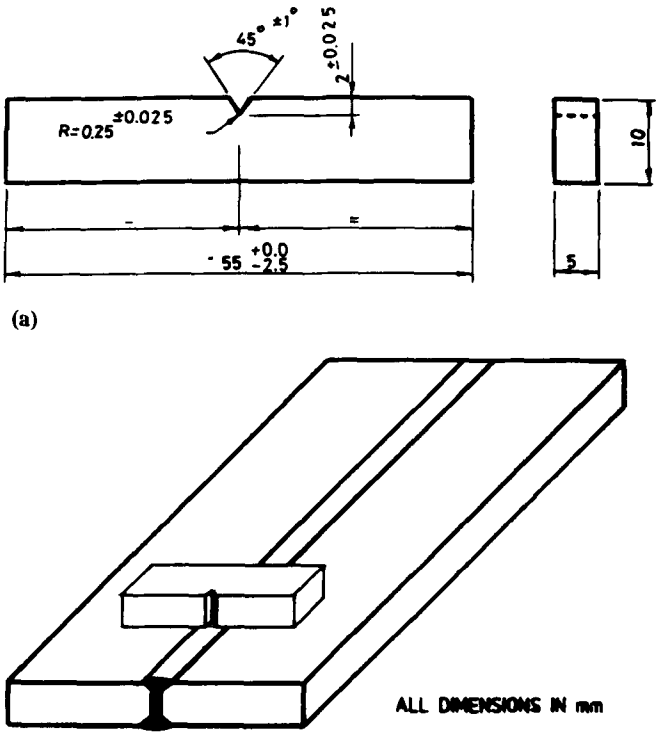

Fig. 12 (a) Dimension of subsize Charpy V-notch specimen used for testing. (b) Orientation of subsize Charpy V-notch weld specimen with respect to weld length

3.7 *Chemical Analysis*

Chemical compositions of the pipe, the dished end, and the weld metal are given in Table 2. Carbon and sulfur contents of pipe and dished-end materials were determined by a combustion method, and a titrametric method was used to estimate the concentrations of phosphorus and manganese. The chemical compositions of the pipe and dished-end materials

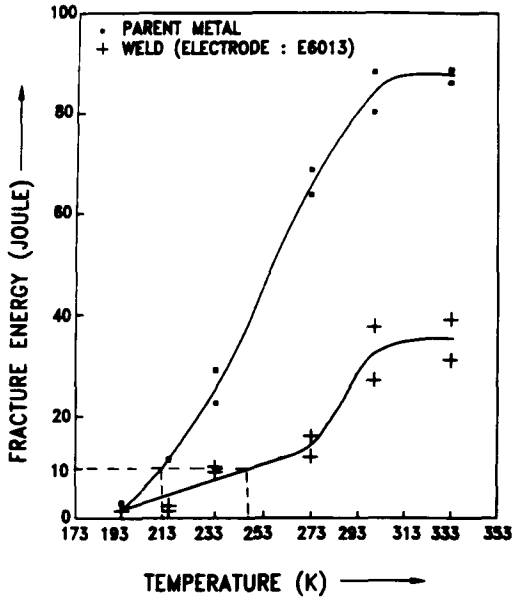

Fig. 13 Plots of absorbed energy versus temperature for subsize Charpy V-notch specimens

conformed to their respective nominal chemical compositions (see Table 1).

4. Discussion

The failed component was constructed of carbon steel with manganese additions of up to 1%. This particular material exhibits ductile-to-brittle transition at subambient temperatures. Low-temperature impact toughness of the weld metal is reported to be poor, especially when the weld metal is made with a cellulose-coated electrode, such as AWS E 6013 (Ref 5, 6). The presence of large amounts of inclusions results in further degradation of the low-temperature impact properties of the weld metal (Ref 7).

Visual examination of the failed component revealed that the weld was nonuniform. The weld joint was poorly designed, with the tapered transition provided at the joint between sections of differing thickness (3 mm) falling well short of the minimum specified limit of 15 mm (Ref 8). Inadequate taper at the weld joint would have resulted in stress concentration at the weld.

Fractographic and metallographic evidence clearly indicated that the failure started at the area of lack of penetration in the weld and propagated in a brittle manner. In the crack initiation zone, cracking was intergranular. This region also exhibited blisters around inclusions. Microcracks emanating from inclusion sites and decohesion of inclusion/matrix interfaces were also noticed.

These features are characteristic of hydrogen embrittlement (Ref 9, 10). According to Towers (Ref 11, 12), for steels with tensile strengths in the range of 334 to 688 MPa, the reduction in testing temperature for subsize Charpy specimens with respect to that for standard specimens can be given by:

$$dT = 0.7(10 - w)^2 \quad \text{(Eq 1)}$$

where dT is the reduction in testing temperature from that required for a standard Charpy V-notch specimen (in degrees Celsius), and w is the specimen width along the notch.

Using Eq 1, the transition temperatures for the base metal and weld metal (20 J criterion for standard Charpy V-notch specimens) have been calculated as 227.5 and 264.5 K, respectively. The mean shift in transition temperatures is likely to differ at most by 12% (Ref 11). The conclusion is that the weld metal is below the ductile to brittle transition temperature when it is at room temperature.

As mentioned earlier, the weld was made with AWS E 6013 electrode, which contains a large amount of cellulose in its coating (Ref 6). At the time of welding, cellulose decomposes into carbon monoxide, carbon dioxide, hydrogen, and other gases, as well as large amounts of steam. The chemical reactions involved are (Ref 13):

$$(C_6H_{10}O_5)_n + (n/2)O_2 = 6nCO + 5nH_2 \quad \text{(Eq 2)}$$

$$2H_2 + O_2 = 2H_2O \quad \text{(Eq 3)}$$

$$C + H_2O = CO + H_2 \quad \text{(Eq 4)}$$

$$H_2 = 2H \quad \text{(Eq 5)}$$

The hydrocarbons emitted during welding volatilize and dissociate to form elemental hydrogen, which dissolves in the weld puddle. As the metal cools from the austenite region, an abrupt drop in hydrogen solubility occurs. In the supersaturated state, the hydrogen diffuses to regions of high stress concentration, where it can initiate a crack (Ref 9).

The area of lack of penetration in the condenser tube weld was a probable stress-concentration site and thus a favorable region for the initiation of hydrogen-induced cracking. Diffusion of hydrogen to an inclusion site results in either decohesion of the inclusion/matrix interface or nucleation of a crack at the inclusion site. Because cracking by hydrogen embrittlement is diffusion controlled, it takes time (in days or months) for the cracking to appear. The maximum susceptibility to hydrogen embrittlement occurs at about room temperature (Ref 14).

It is believed that hydrogen-induced cracking took place during storage of the component after welding. It did not result in failure during hydrotesting, however, because the crack length was smaller than the critical crack length at room temperature. As the weld was associated with poor low-temperature impact properties, lowering the temperature of the component during startup facilitated growth of the crack developed during storage (under the combined influence of operating and residual stresses). This culminated in catastrophic failure as soon as the crack reached critical length.

5. Conclusions

In view of the evidence gathered during the investigation, the sequence of events preceding failure can be outlined as follows:

- The weld region of the condenser tube component was associated with an area of lack of penetration throughout most of the weld length.
- Hydrogen absorbed at the time of welding assisted crack initiation from the area of lack of penetration (a stress-concentration site) under the possible influence of weld residual stresses. This is believed to have taken place at room temperature during storage of the component after welding.
- Poor weld toughness at the low operating temperature facilitated crack growth during startup, culminating in catastrophic failure as soon as the crack attained critical length.

Acknowledgments

The authors are grateful to Dr. Placid Rodriguez, Director of IGCAR, for constant encouragement and support. They also wish to thank P. Sukumar, N. Raghu, S. Kartic Babu, and M. Radhika for their help during various stages of this investigation.

References

1. *Metals and Alloys in the Unified Numbering System,* 4th ed., Society of Automotive Engineers, 1986, p 127
2. *Metals Handbook,* Vol 1, *Properties and Selection of Irons and Steels,* 9th ed., American Society for Metals, 1983, p 318-319, 320-321, 692-693
3. "Standard Methods for Notched Bar Impact Testing of Metallic Materials," E 23, *Annual Book of ASTM Standards,* Part 10, ASTM, 1980, p 197-212
4. Standard Methods for Mechanical Testing of Welds, ANSI/AWS B 4.0-85, American Welding Society, Florida, 1985, p 31-37
5. J.F. Lancaster, *Metallurgy of Welding,* 3rd ed., George Allen & Unwin, London, 1980, p 128-129
6. *Metals Handbook,* Vol 1, *Properties and Selection of Metals,* 8th ed., American Society for Metals, 1961, p 338-340, 343-344
7. *Metals Handbook,* Vol 6, *Welding, Brazing, and Soldering,* 9th ed., American Society for Metals, 1983, p 12
8. "ASME Boiler and Pressure Vessel Code," Section VIII, Div. 1, "Requirement for Pressure Vessels Fabricated by Welding," American Society of Mechanical Engineers, 1992, p 105-108
9. *Metals Handbook,* Vol 10, *Failure Analysis and Prevention,* 8th ed., American Society for Metals, 1975, p 231, 335
10. *Failure Analysis: The British Engine Technical Reports,* F.R. Hutching and P.M. Unterweiser, Ed., American Society for Metals, 1981, p 40-41
11. O.L. Towers, Charpy Requirements for Sub-size Specimens, *Weld. Inst. Res. Bull.,* Vol 19 (No. 8), 1978, p 224-227
12. O.L. Towers, Testing Sub-size Charpy Specimens: Part I—The Influence of Thickness on the Ductile/Brittle Transition, *Met. Constr.,* Vol 18 (No. 3), 1986, p 171R-176R
13. H. Udin, E.R. Funk, and J. Wulf, *Welding for Engineers,* John Wiley & Sons, London, 1954, p 186
14. C.L. Briant, *Metallurgical Aspects of Environmental Failure,* Elsevier Science, 1985, p 71-92